INTERNATIONAL JOURNAL FOR NUMERICAL METHODS IN FLUIDS, VOL. 12, 161–177 (1991)

ASSESSMENT OF TVD SCHEMES FOR INVISCID AND TURBULENT FLOW COMPUTATION

MING-HSIUNG CHEN, CHEN-CHI HSU AND WEI SHYY

Department of Aerospace Engineering, Mechanics and Engineering Science, University of Florida, Gainesville, Florida 32611, U.S.A.

SUMMARY

A systematic study has been conducted to assess the performance of the TVD schemes for practical flow computation. The viewpoint adopted here is to treat the TVD schemes as a combination of the standard central difference scheme with numerical dissipation terms. The controlled amount of numerical dissipation modifies the computed fluxes to ensure that the solution is oscillation-free. Four variants of TVD schemes, two with upwind dissipation terms and two with symmetric dissipation terms, have been studied and compared with the conventional Beam–Warming scheme for inviscid and turbulent axisymmetric flow computations. The results obtained show that all four variants can accurately resolve the shock and flow profiles with fewer grid points than the Beam–Warming scheme. The convergence rates of the TVD schemes are also substantially superior to that of the Beam–Warming scheme. The combination of high accuracy, good robustness and improved computational efficiency offered by the TVD schemes makes them attractive for computing high-speed flow with shocks. In terms of the relative performances it is found that the symmetric schemes converge slightly faster but that the upwind schemes are less sensitive to the number of grid points being employed.

KEY WORDS Convection approximation Total variation diminishing schemes Shock Turbulent and inviscid flows

1. INTRODUCTION

Recently, a number of new techniques for constructing non-linear, high-resolution shock-capturing schemes for systems of hyperbolic conservation laws have been developed.[1–10] These schemes, characterized by the total-variation-diminishing (TVD) property, are free from generating spurious oscillations across the regions of sharp flow profile such as shocks and contact discontinuities, and can converge to physically realizable solutions with the aid of entropy correction. In the region of smoothly varying solutions the TVD schemes can also maintain a high degree of numerical accuracy.

The TVD concept was first proposed by Harten[3] who also developed a simple algebraic criterion for constructing first-order-accurate TVD schemes. He then added a limited antidiffusive flux to a first-order-accurate entropy-satisfying scheme to obtain the second-order-accurate TVD schemes. This technique is referred as the 'modified flux approach'. The modified flux is devised so that the scheme is second-order-accurate in the smooth region and will switch itself to first-order accuracy in the vicinity of points of extrema. Harten[4] also extended a class of explicit TVD schemes to a more general category which includes a one-parameter family of implicit second-order TVD schemes. More recently, Harten's TVD scheme was modified and generalized by Yee *et al.*[8] and implemented to solve the two-dimensional Euler equations of gasdynamics for

0271–2091/91/020161–17$08.50 *Received 6 April 1989*

the aerofoil problem. The numerical results indicate that Harten's scheme is both robust and accurate.

Van Leer[5] adopted an approach originally developed by Godunov,[11] who used a control volume concept to ensure the numerical scheme to be conservative and therefore dealt with averaged values instead of nodal values in each finite volume. Van Leer observed that it is beneficial to work with averaged gradients in addition to averaged values, i.e. one can obtain second-order accuracy by replacing the piecewise-constant initial data of the Riemann problem of Godunov's scheme with the piecewise-linear initial data. The slope of the piecewise-linear initial data is selected so that spurious oscillations will be prevented. Colella and Woodward[6] further refined van Leer's idea by using piecewise-parabolic initial data and have obtained remarkably good numerical solutions.

Roe[12–14] has developed a numerical fluctuation approach for computing the numerical solution of both scalar and systems of hyperbolic conservation laws. His approach combines a novel interpretation of difference schemes with higher-order accuracy and monotonicity preservation and also incorporates these properties into an approximate Riemann solver for hyperbolic systems. The average function is constructed by the use of flux limiters. Using this approach, Roe has obtained solutions with crisp shock free from the spurious oscillations. Unfortunately, Roe's scheme may also admit a non-physical (entropy-violating) solution, i.e. expansion shock. Various remedies have been proposed to cure this problem.[15–17]

Osher has constructed a scheme[18] based on an approximate Riemann solver, with the use of compression and rarefaction waves to approximate shocks. The numerical flux functions, which are at least continuously differentiable, are written in closed form and include various switches which make the numerical flux functions upwind, and the numerical solutions satisfy the entropy condition. It is observed that Osher's scheme require more operations than Harten's or van Leer's scheme.[19]

Davis[20] showed that a certain class of TVD schemes can be interpreted as a Lax–Wendroff scheme plus an upwind-weighted conservative numerical dissipation term. He then simplified the scheme by eliminating the upwind weight of this numerical dissipation term and also ensured that the simplified scheme still possesses the TVD properties. Roe[21] reformulated Davis's scheme to make it easier to analyse. He also formulated a class of TVD schemes not obtained by Davis. Yee[9] then generalized Roe's schemes to a one-parameter family of second-order explicit and implicit TVD schemes. Therefore the formulation of Roe and Davis's scheme can simply be viewed as special cases of Yee's explicit symmetric TVD schemes.

In the present study, several of the aforementioned TVD schemes are analysed and compared in the context of practical flow computation. The viewpoint of interpreting the TVD scheme as a modified flux is adopted here in order to make the task of actual implementation of several different schemes more tractable. One can modify a standard three-point central difference code such as the Beam–Warming algorithm[22] by simply changing the conventional dissipation terms into the one designed for the TVD schemes. Hence the only difference in computation is that the TVD scheme requires more elaborate dissipation terms or flux limiters.

An extended derivation of the TVD schemes in three-dimensional generalized curvilinear coordinates has been presented in Reference 23. This formula has been applied to actual flow computations by incorporating it into a time-dependent axisymmetric Navier–Stokes formulation based on the Beam–Warming scheme. Both inviscid and turbulent flows over the axisymmetric secant–ogive–cylinder–boat-tailed (SOCBT) projectile with string at zero angle of attack have been computed. The goal is to assess the performance of the TVD schemes in terms of numerical accuracy, robustness and convergence rate. Four variants of the TVD scheme have been investigated in the present study, namely two upwind schemes with flux limiters proposed by

van Leer[5] and Roe[2] respectively, and two symmetric schemes originally developed by Roe and Davis and later extended by Yee.[9]

2. GOVERNING EQUATIONS AND NUMERICAL ALGORITHM

The azimuthal-invariant thin layer Navier–Stokes equations in general curvilinear co-ordinates[24,25] can be written as

$$\frac{\partial \hat{q}}{\partial \tau}+\frac{\partial \hat{E}}{\partial \xi}+\frac{\partial \hat{G}}{\partial \zeta}=\frac{1}{Re}\frac{\partial \hat{S}}{\partial \zeta}+\hat{H}. \tag{1}$$

Here

$$\hat{q}=J^{-1}\begin{bmatrix}\rho\\ \rho u\\ \rho v\\ \rho w\\ e\end{bmatrix}, \qquad \hat{E}=J^{-1}\begin{bmatrix}\rho U\\ \rho uU+\xi_x p\\ \rho vU\\ \rho wU+\xi_z p\\ (e+p)U-\xi_t p\end{bmatrix},$$

$$\hat{G}=J^{-1}\begin{bmatrix}\rho W\\ \rho uW+\zeta_x p\\ \rho vW\\ \rho wW+\zeta_z p\\ (e+p)W-\zeta_t p\end{bmatrix}, \quad \hat{S}=J^{-1}\begin{bmatrix}0\\ m_1 u_\zeta+m_2\zeta_x\\ m_1 v_\zeta\\ m_1 w_\zeta+m_2\zeta_z\\ m_1 m_3+m_2(\zeta_x u+\zeta_z w)\end{bmatrix},$$

$$\hat{H}=J^{-1}\begin{bmatrix}0\\ 0\\ \rho V[R_\xi(U-\xi_t)+R_\zeta(W-\zeta_t)]\\ -\rho VR(V-\eta_t)-p/R\\ 0\end{bmatrix}$$

and

$$m_1=\mu(\zeta_x^2+\zeta_z^2), \qquad m_2=(\mu/3)(\zeta_x u_\zeta+\zeta_z w_\zeta),$$
$$m_3=(u^2+v^2+w^2)_\zeta/2+\mu Pr^{-1}(\gamma-1)^{-1}(c^2)_\zeta,$$
$$U=\xi_t+\xi_x u+\xi_z w, \qquad V=\eta_t+\eta_y v, \qquad W=\zeta_t+\zeta_x u+\zeta_z w,$$

where ρ, u, v, w, p and e are the density, velocity components along the x-, y- and z-directions, static pressure and total energy respectively; μ, γ, c and Pr are the dynamic viscosity, ratio of specific heats, speed of sound and Prandtl number respectively. The co-ordinate transformation between (x, y, z) and (ξ, η, ζ) is made with U, V and W being the contravariant velocity components.

In order to highlight the influence of the TVD schemes on the numerical algorithm, the widely adopted Beam–Warming scheme[22] is used as the base method. In the present framework the major difference between the Beam–Warming scheme and the TVD schemes can be interpreted in terms of the dissipation mechanism. The Beam–Warming scheme is a non-iterative approximate factorization implicit algorithm. The finite difference equation resulting from the Beam–Warming scheme for approximating equation (1) can be expressed as

$$L_\xi L_\zeta[\Delta\hat{q}^n]=-\Delta t(\delta_\xi \hat{E}^n+\delta_\zeta \hat{G}^n-Re^{-1}\delta_\zeta \hat{S}^n+\hat{H}^n)-D_e, \tag{2}$$

with the linear operators L_ξ and L_ζ defined as

$$L_\xi = [I + \Delta t \delta_\xi \hat{A}^n - D_i|_\xi], \tag{3}$$

$$L_\zeta = [I + \Delta t \delta_\zeta \hat{C}^n - \Delta t Re^{-1} \delta_\zeta J^{-1} \hat{M}^n J - D_i|_\zeta], \tag{4}$$

where the explicit fourth-order dissipation is

$$D_e = \varepsilon_e \Delta t J^{-1} [(\Delta_\xi \nabla_\xi)^2 + (\Delta_\zeta \nabla_\zeta)^2] J \tag{5}$$

and the implicit second-order dissipation terms are

$$D_i|_\xi = \varepsilon_i \Delta t J^{-1} (\Delta \nabla)_\xi J, \tag{6}$$

$$D_i|_\zeta = \varepsilon_i \Delta t J^{-1} (\Delta \nabla)_\zeta J. \tag{7}$$

Here δ is a standard three-point second-order-accurate central difference operator, Δ and ∇ are forward and backward-difference operators respectively and J is the Jacobian of the co-ordinate transformations. The Jacobian matrices $\hat{A}$, $\hat{C}$ and $\hat{M}$ result from the linearization of the flux vectors $\hat{E}$, $\hat{G}$ and $\hat{S}$ respectively, i.e. $\hat{A} = \partial \hat{E}/\partial \hat{q}$, $\hat{C} = \partial \hat{G}/\partial \hat{q}$ and $\hat{M} = \partial \hat{S}/\partial \hat{q}$. The parameters ε_i and ε_e are chosen such that $\varepsilon_i \geq 2\varepsilon_e$. Specifically, the dissipation terms due to the Beam–Warming scheme in equations (5)–(7) can now be replaced by the following expressions:

$$D_e = -\tfrac{1}{2}\Delta t(R_{i+1/2}\Phi_{i+1/2} - R_{i-1/2}\Phi_{i-1/2} + R_{k+1/2}\Phi_{k+1/2} - R_{k-1/2}\Phi_{k-1/2}) \tag{8}$$

and

$$D_i|_\xi = -\tfrac{1}{2}\Delta t(\Omega^\xi_{i+1/2,k} - \Omega^\xi_{i-1/2,k}), \tag{9}$$

$$D_i|_\zeta = -\tfrac{1}{2}\Delta t(\Omega^\zeta_{i,k+1/2} - \Omega^\zeta_{i,k-1/2}), \tag{10}$$

where $R_\xi = (R^1_\xi, R^2_\xi, R^3_\xi, R^4_\xi, R^5_\xi)$ and $R_\zeta = (R^1_\zeta, R^2_\zeta, R^3_\zeta, R^4_\zeta, R^5_\zeta)$, the matrices whose columns are eigenvectors of $\hat{A}$ and $\hat{C}$, are defined as

$$R_\kappa = \begin{bmatrix} \tilde{\kappa}_x & \tilde{\kappa}_y & \tilde{\kappa}_z & 1 & 1 \\ \tilde{\kappa}_x u & \tilde{\kappa}_y u - \tilde{\kappa}_z \rho & \tilde{\kappa}_z u + \tilde{\kappa}_y \rho & u + \tilde{\kappa}_x c & u - \tilde{\kappa}_x c \\ \tilde{\kappa}_x v + \tilde{\kappa}_z \rho & \tilde{\kappa}_y v & \tilde{\kappa}_z v - \tilde{\kappa}_x \rho & v + \tilde{\kappa}_y c & v - \tilde{\kappa}_y c \\ \tilde{\kappa}_x w - \tilde{\kappa}_y \rho & \tilde{\kappa}_y w + \tilde{\kappa}_x \rho & \tilde{\kappa}_z w & w + \tilde{\kappa}_z c & w - \tilde{\kappa}_z c \\ \tilde{\kappa}_x q^2/2 + \rho(\tilde{\kappa}_z v - \tilde{\kappa}_y w) & \tilde{\kappa}_y q^2/2 + \rho(\tilde{\kappa}_x w - \tilde{\kappa}_z u) & \tilde{\kappa}_z q^2/2 + \rho(\tilde{\kappa}_y u - \tilde{\kappa}_x v) & H + c\tilde{\theta} & H - c\tilde{\theta} \end{bmatrix}, \tag{11}$$

with $\kappa = \xi$, η or ζ and $R_{i+1/2}$ denoting R_ξ evaluated at $q_{i+1/2,k}$,

$$R_\kappa^{-1} = \begin{bmatrix} \tilde{\kappa}_x(1-b_1) - (\tilde{\kappa}_z v - \tilde{\kappa}_y w)/\rho & \tilde{\kappa}_x b_2 u & \tilde{\kappa}_z/\rho + \tilde{\kappa}_x b_2 v & -\tilde{\kappa}_y/\rho + \tilde{\kappa}_x b_2 w & -\tilde{\kappa}_x b_2 \\ \tilde{\kappa}_y(1-b_1) - (\tilde{\kappa}_x w - \tilde{\kappa}_z u)/\rho & -\tilde{\kappa}_z/\rho + \tilde{\kappa}_y b_2 u & \tilde{\kappa}_y b_2 v & \tilde{\kappa}_x/\rho + \tilde{\kappa}_y b_2 w & -\tilde{\kappa}_y b_2 \\ \tilde{\kappa}_z(1-b_1) - (\tilde{\kappa}_y u - \tilde{\kappa}_x v)/\rho & \tilde{\kappa}_y/\rho + \tilde{\kappa}_z b_2 u & -\tilde{\kappa}_x/\rho + \tilde{\kappa}_z b_2 v & \tilde{\kappa}_z b_2 w & -\tilde{\kappa}_z b_2 \\ (b_1 - \tilde{\theta}/c)/2 & (\tilde{\kappa}_x/c - b_2 u)/2 & (\tilde{\kappa}_y/c - b_2 v)/2 & (\tilde{\kappa}_z/c - b_2 w)/2 & b_2/2 \\ (b_1 + \tilde{\theta}/c)/2 & -(\tilde{\kappa}_x/c + b_2 u)/2 & -(\tilde{\kappa}_y/c + b_2 v)/2 & -(\tilde{\kappa}_z/c + b_2 w)/2 & b_2/2 \end{bmatrix}, \tag{12}$$

where

$$\tilde{\kappa}_x = \kappa_x/(\kappa_x^2+\kappa_y^2+\kappa_z^2)^{1/2}, \quad \tilde{\kappa}_y = \kappa_y/(\kappa_x^2+\kappa_y^2+\kappa_z^2)^{1/2}, \quad \tilde{\kappa}_z = \kappa_z/(\kappa_x^2+\kappa_y^2+\kappa_z^2)^{1/2},$$

$$\tilde{\theta} = \tilde{\kappa}_x u + \tilde{\kappa}_y v + \tilde{\kappa}_z w, \quad q^2 = u^2+v^2+w^2, \quad H = c^2/(\gamma-1)+q^2/2,$$

$$b_1 = b_2(q^2/2), \quad b_2 = (\gamma-1)/c, \quad c = (\gamma p/\rho)^{1/2}.$$

The elements of $\Phi_{i+1/2}$ denoted by $(\Phi^l_{i+1/2})^{\mathrm{U}}$ for a second-order upwind TVD scheme, originally developed by Harten[3] and later modified and generalized by Yee *et al.*,[8] are

$$(\phi^l_{i+1/2})^{\mathrm{U}} = \sigma(a^l_{i+1/2})(g^l_{i+1}-g^l_i) - \psi(a^l_{i+1/2}+\gamma^l_{i+1/2})\alpha^l_{i+1/2}. \tag{13}$$

Here

$$\sigma(z) = \tfrac{1}{2}\psi(z)$$

and the coefficient of numerical viscosity can be slightly modified as

$$\psi(z) = \begin{cases} |z|, & |z| \geq \varepsilon, \\ (z^2+\varepsilon^2)/2\varepsilon, & |z| < \varepsilon, \end{cases}$$

where ε is a small positive parameter.

The function γ is defined as

$$\gamma^l_{i+1/2} = \sigma(a^l_{i+1/2}) \begin{cases} (g^l_{i+1}-g^l_i)/\alpha^l_{i+1/2}, & \alpha^l_{i+1/2} \neq 0, \\ 0, & \alpha^l_{i+1/2} = 0. \end{cases}$$

The characteristic variables $\alpha_{i+1/2,k}$ and $\alpha_{i,k+1/2}$ can be expressed as

$$\alpha^l_{i+1/2} = \frac{R^{-1}_{i+1/2}(q_{i+1,k}-q_{i,k})}{\frac{1}{2}(J_{i+1,k}+J_{i,k})},$$

$$\alpha^l_{k+1/2} = \frac{R^{-1}_{k+1/2}(q_{i,k+1}-q_{i,k})}{\frac{1}{2}(J_{i,k+1}+J_{i,k})}.$$

The symbol g^l_i represents the 'flux limiter', which has been proposed to be of the following forms.

(i) Harten's flux limiter:[3]

$$g^l_i = \text{minmod}\,(\alpha^l_{i-1/2}, \alpha^l_{i+1/2}), \tag{14a}$$

where the minmod function of two arguments is defined as

$$\text{minmod}\,(x, y) = \text{sgn}(x)\max\{0, \min[|x|, y\,\text{sgn}(x)]\}.$$

(ii) Van Leer's flux limiter:[26]

$$g_i = (\alpha^l_{i+1/2}\alpha^l_{i-1/2} + |\alpha^l_{i+1/2}\alpha^l_{i-1/2}|)/(\alpha^l_{i+1/2}+\alpha^l_{i-1/2}). \tag{14b}$$

(iii) Roe's flux limiter:[2]

$$g^l_i = S\max[0, \min(2|\alpha^l_{i+1/2}|, S\alpha^l_{i-1/2}), \min(|\alpha^l_{i+1/2}|, 2S\alpha^l_{i-1/2})], \tag{14c}$$

with

$$S = \text{sign}\,(\alpha^l_{i+1/2}).$$

Flux limiter (14c) is found to produce the most compressive, i.e. stiff, profile among the three limiters. Limiter (14b) is found to produce better shock resolution than (14a).[9]

The elements of $\Phi_{i+1/2}$ denoted by $(\phi^l_{i+1/2})^S$ for a general second-order symmetric TVD scheme[9] are

$$(\phi^l_{i+1/2})^S = -\psi(a^l_{i+1/2})\,[\alpha^l_{i+1/2} - \hat{Q}^l_{i+1/2}]. \tag{15}$$

Again $\hat{Q}^l_{i+1/2}$ is the flux limiter, which can be either of the following forms, for example.

(iv) Davis's flux limiter:[20]

$$\hat{Q}^l_{i+1/2} = \text{minmod}(\alpha^l_{i-1/2}, \alpha^l_{i+1/2}) + \text{minmod}(\alpha^l_{i+1/2}, \alpha^l_{i+1/2}) - \alpha^l_{i+1/2}. \tag{16a}$$

(v) Yee–Roe–Davis's flux limiter:[9,21]

$$\hat{Q}^l_{i+1/2} = \text{minmod}[2\alpha^l_{i-1/2}, 2\alpha^l_{i+1/2}, 2\alpha^l_{i+1/2}, \tfrac{1}{2}(\alpha^l_{i-1/2} + \alpha^l_{i+1/2})]. \tag{16b}$$

Limiter (16b) is more compressive than limiter (16a).[9]

Finally, $\Omega^\xi_{i+1/2,k}$ and $\Omega^\zeta_{i,k+1/2}$ in equations (9) and (10) can be expressed as

$$\Omega^\xi_{i+1/2,k} = \text{diag}\left[-\max_l \psi(a^l_{i+1/2})\right]\Delta_{i+1/2},$$

$$\Omega^\zeta_{i,k+1/2} = \text{diag}\left[-\max_l \psi(a^l_{k+1/2})\right]\Delta_{k+1/2}.$$

In the present work, four different limiters, two upwind schemes and two symmetric schemes, have been adopted to study the performance of the TVD schemes. The two upwind TVD schemes are one proposed by van Leer, as shown in equation (14b), and the other a combination of van Leer's limiter, equation (14b) for the non-linear characteristic field and of Roe's limiter, equation (14c), for the linear characteristic field. The two symmetric limiters are those expressed in equations (16a) and (16b).

3. NUMERICAL RESULTS AND DISCUSSION

The transonic flow over the axisymmetric SOCBT projectile with sting at zero angle of attack with $M_\infty = 0{\cdot}96$ and $1{\cdot}2$ are used as test cases. The projectile model used in the computation is shown in Figure 1(a) and consists of three-calibre for the secant–ogive part, two-calibre for the cylinder part and one-calibre, 7° for the boat-tail part, which is further extended for another 1·77 calibre to meet straight sting. Both turbulent and inviscid flows have been computed to contrast the solutions yielded by different numerical schemes on the one hand and to compare the difference between the inviscid and turbulent flows on the other hand. The differences in convergence rates of the various schemes and flow regimes will also be studied. The Baldwin–Lomax algebraic mixing length model[27] has been adopted here as the turbulence closure.

A 90×60 'C-type' grid system was generated using a hyperbolic solver[28] as shown in Figure 1(b). An expanded view of the grid near the projectile is shown in Figure 1(c). The grid points are clustered near the ogive–cylinder and cylinder–boat-tail junctions in the streamwise (ξ-) direction. In the cross-stream direction, i.e. the ζ-direction, the grid points are exponentially clustered near the body surface with a minimum spacing of 2×10^{-5} diameters to resolve the viscous sublayer. In order to isolate the factors contributing to the change of numerical solutions, identical grid systems will be used for both turbulent and inviscid flows.

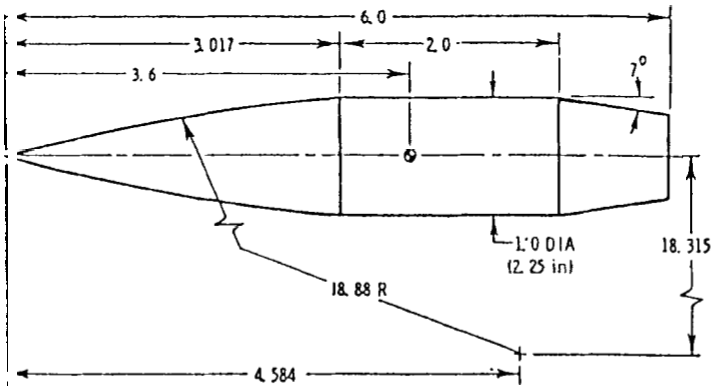

Figure 1(a). Configuration of the secant–ogive–cylinder–boat-tail (SOCBT) projectile

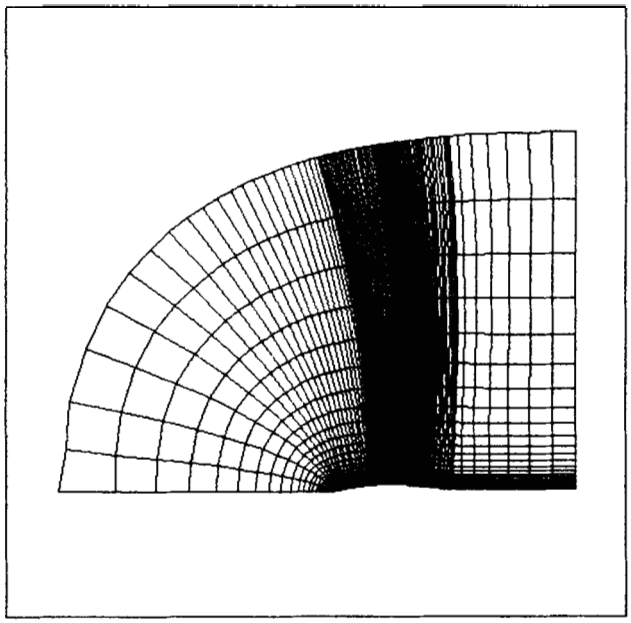

Figure 1(b). A 90 × 60 'C' grid system for the SOCBT projectile

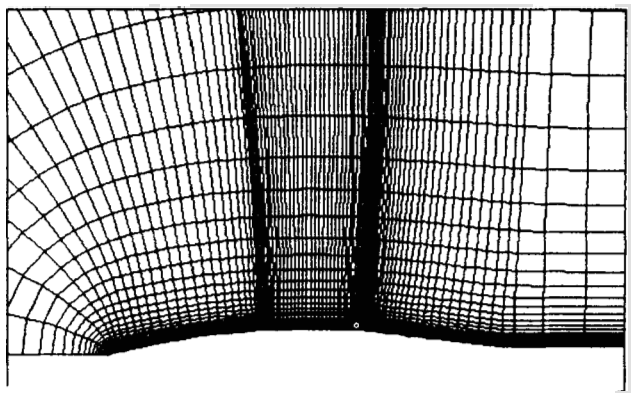

Figure 1(c). Expanded view of the grid distribution near the projectile

3.1. $M_\infty = 0{\cdot}96$

Figure 2 shows the steady state solutions of surface pressure coefficient C_p and Mach contours of inviscid as well as turbulent flows calculated by the Beam–Warming scheme. In Figure 2(a) the open symbols indicate the wind tunnel experimental data obtained by Kayser and Whiton[29] while the solid and dotted lines represent the numerical solutions of the turbulent and inviscid flows respectively. Corresponding results obtained by the TVD schemes are presented in Figures 3–6. After inspecting the results obtained by the various numerical schemes, the following observations can be made.

(i) With the size and distribution of the present grid system, the pressure coefficients along the projectile predicted by all schemes agree closely with each other for both the turbulent and inviscid flows.

(ii) There are visible differences in the predicted pressure coefficients between the turbulent flow and the inviscid flow. The pressure coefficient in the inviscid flow invariably depicts steeper slopes than that of the turbulent flow. This behaviour is expected since the viscous effects smear out the sharp variations of the flow field. The inviscid solutions are able to agree more closely with a peak value of experimental measurement located in the shock region above the middle of the cylinder segment. However, the turbulent results agree substantially better in the region of the second shock, where the inviscid solutions show too steep a profile. The difference is most likely caused by the interaction of shock and turbulent boundary layer which, as demonstrated in the Mach contours, modifies the effective wall contours, especially in the region after the second shock.

(iii) Although the agreements among the numerical results obtained by the various schemes are very good for the surface pressure coefficient, differences exist in terms of the detailed flow field, as demonstrated by the Mach contours. The flow field predicted by the Beam and Warming scheme is much more smeared than those by the TVD schemes because of the larger amount of numerical dissipation being introduced into the discrete equations.

(iv) With regard to the performance of the TVD schemes, they all yield essentially identical results. Overall, excellent agreements have been observed among all the TVD schemes with the present grid system. Only Davis's symmetric scheme, i.e. equation (16a), shows some discrepancies between the experimental and predicted values of C_p in the region before the first shock. Figure 7 compares the convergence rates among the Beam–Warming scheme and the four TVD schemes for both the inviscid and turbulent flows with the grid system shown in Figure 1.

The following comments can be made with respect to the relative performances of the schemes under study.

(i) As expected, the convergence rates of the inviscid flow calculations are faster than those of the turbulent calculations for all the schemes.

(ii) The Beam–Warming scheme shows considerably slower convergence rates than all the TVD schemes for both the inviscid and turbulent flows. In the present formulation the CPU time per iteration required by the Beam–Warming scheme is a little shorter than the TVD schemes, ranging from 15% to 30%. By combining the performance of convergence rate and CPU time requirement per iteration, however, it is clear that all four variants of the TVD scheme are superior to the Beam–Warming scheme in terms of overall computational efficiency.

(iii) Among the TVD schemes, the two symmetric limiters show both faster convergence rates and less CPU time requirements per iteration than the upwind schemes. It was found that

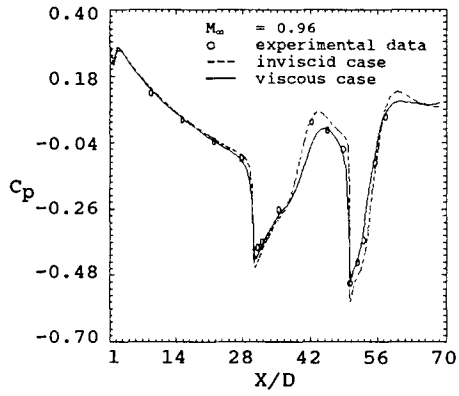

(a) pressure coefficients.

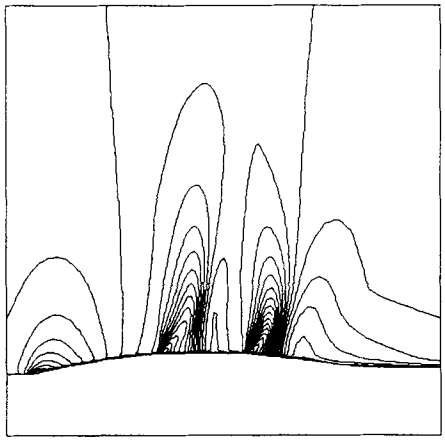

(b) Mach contours of inviscid flow.

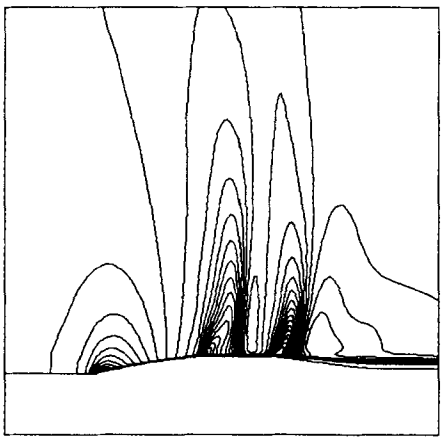

(c) Mach contours of turbulent flow.

Figure 2. Solutions of inviscid and turbulent flows computed by Beam–Warming scheme for $M_\infty = 0{\cdot}96$ using 90×60 grids

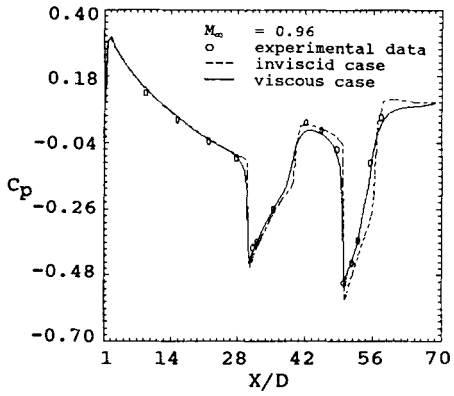

(a) pressure coefficients.

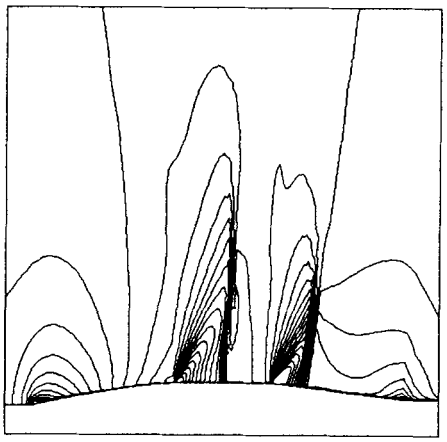

(b) Mach contours of inviscid flow.

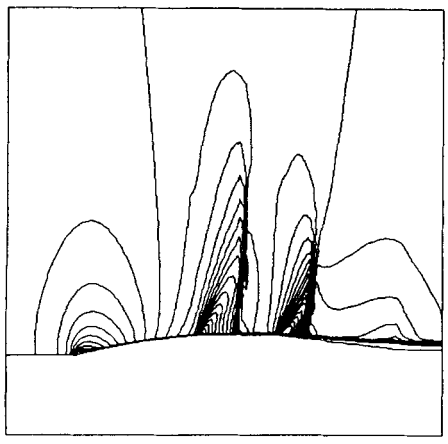

(c) Mach contours of turbulent flow.

Figure 3. Solutions of inviscid and turbulent flows computed by TVD scheme with van Leer's upwind limiter for $M_\infty = 0{\cdot}96$ using 90×60 grids

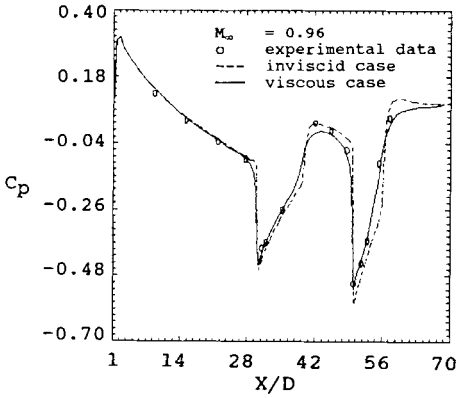

(a) pressure coefficients.

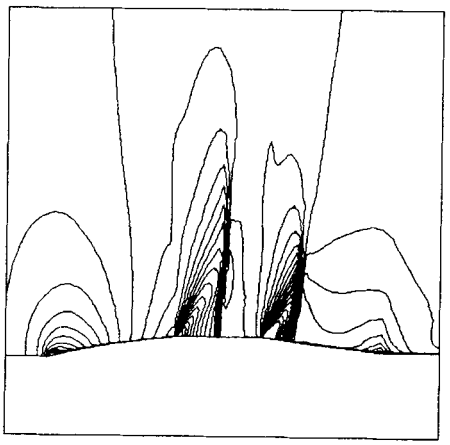

(b) Mach contours of inviscid flow.

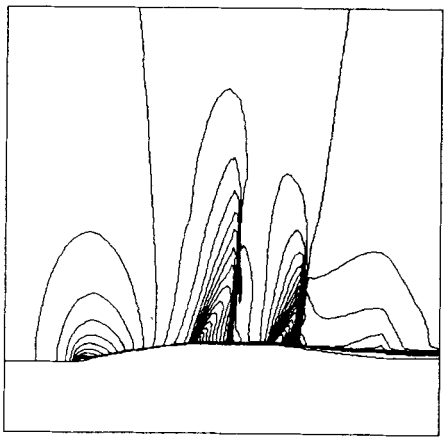

(c) Mach contours of turbulent flow.

Figure 4. Solutions of inviscid and turbulent flows computed by TVD scheme with van Leer's and Roe's combined limiter for $M_\infty = 0{\cdot}96$ using 90×60 grids

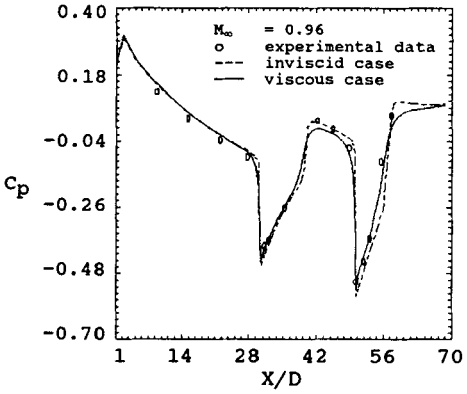

(a) pressure coefficients.

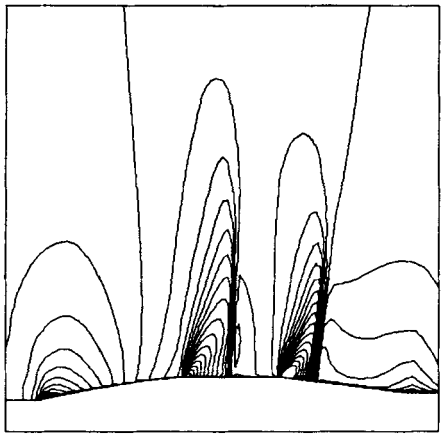

(b) Mach contours of inviscid flow.

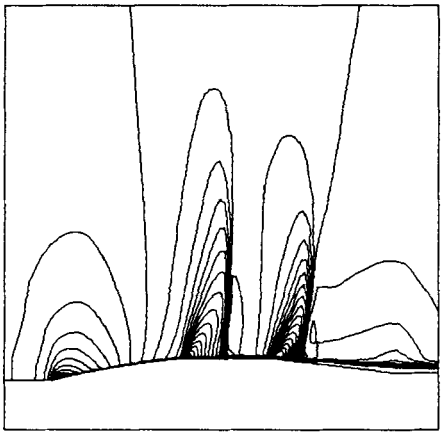

(c) Mach contours of turbulent flow.

Figure 5. Solutions of inviscid and turbulent flows computed by TVD scheme with Davis's symmetric limiter for $M_\infty = 0{\cdot}96$ using 90×60 grids

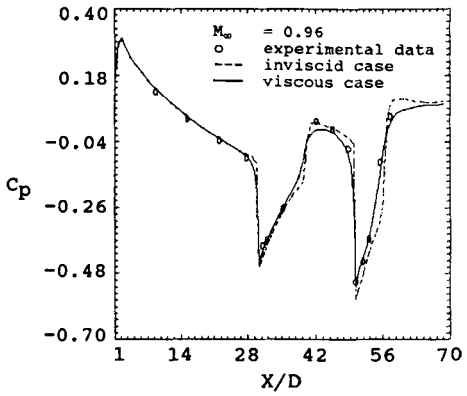

(a) pressure coefficients.

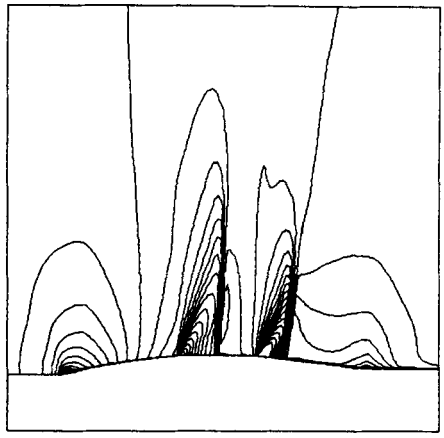

(b) Mach contours of inviscid flow.

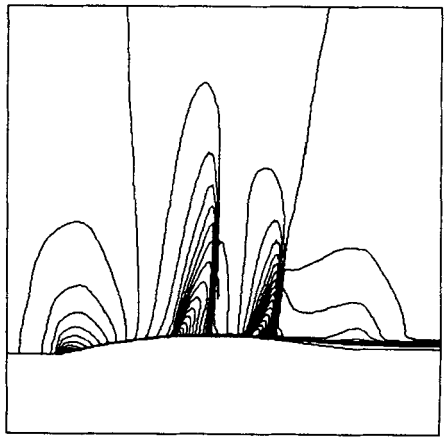

(c) Mach contours of turbulent flow.

Figure 6. Solutions of inviscid and turbulent flows computed by TVD scheme with Yee–Roe–Davis's symmetric limiter for $M_\infty = 0{\cdot}96$ using 90×60 grids

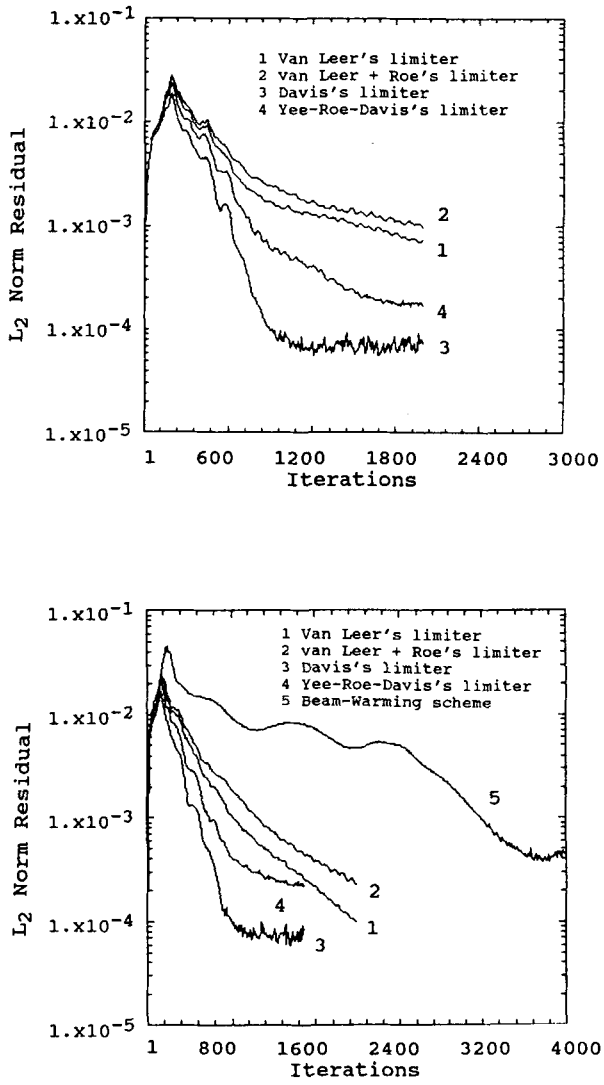

Figure 7. Convergence histories of Beam–Warming scheme and four TVD schemes for $M_\infty = 0{\cdot}96$ with 90×60 grids

both symmetric TVD schemes require about the same amount of CPU time for the present calculations. Their CPU time requirement is about 10% less than that of the van Leer scheme and about 15% less than that of the combined van Leer–Roe scheme. Hence the symmetric TVD schemes appear more attractive for the flows with the present grid system.

It should also be emphasized that another advantage of the TVD schemes is that a user does not have to resort to empirical rules to choose the dissipation parameters. In the Beam–Warming scheme the proper choices of the free parameters such as ε_i and ε_e are not always clear; a trial-and-error approach is usually needed in order to compromise the numerical stability and accuracy. On the other hand, the TVD schemes do not need any free parameters in determining the desirable numerical dissipation.

In order to investigate the effects of the grid distribution on the performances of various schemes, the number of grid points along the transverse (ζ-) direction is reduced from 60 to 40. The solutions obtained by all four TVD schemes are again essentially the same. Figures 8 and 9 compare the pressure coefficients and Mach contours of the turbulent case predicted by the Beam–Warming and the van Leer limiter respectively on the 90 × 40 grid system. The Beam–Warming scheme fails to capture the shock adequately and its accuracy is much inferior to the results obtained using the TVD scheme. The TVD schemes produce indistinguishable results on both the 90 × 60 and 90 × 40 grid systems. The capability of the TVD schemes to accurately resolve the fast variations of the flow field is thus clearly demonstrated through the grid reduction procedure.

To compare the performances among the four limiters of the TVD scheme under study, it was decided to further reduce the number of grid points to 70 × 40. The pressure coefficients and

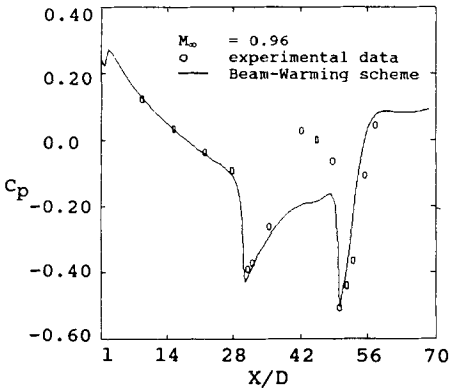

(a) pressure coefficients.

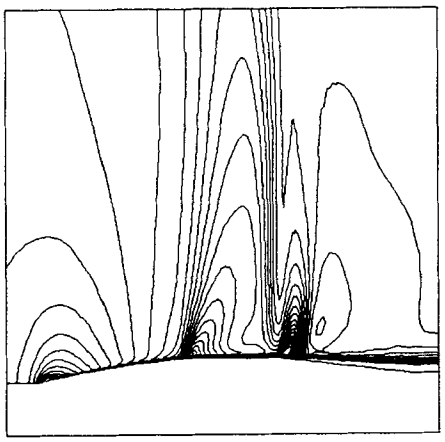

(b) Mach contours of turbulent flow.

Figure 8. Solutions of turbulent flow computed by Beam–Warming scheme for $M_\infty = 0{\cdot}96$ with 90×40 grids

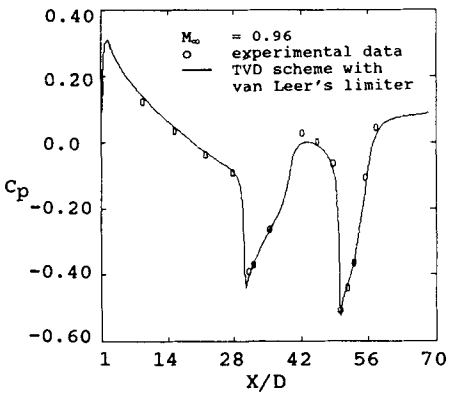

(a) pressure coefficients.

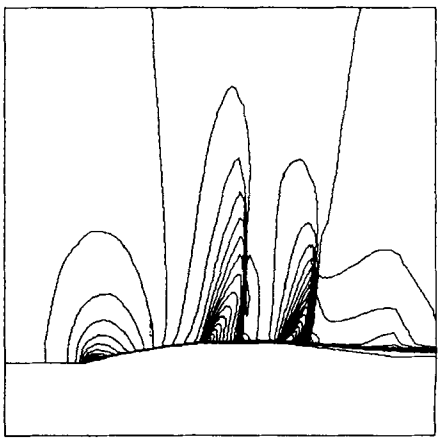

(c) Mach contours of turbulent flow.

Figure 9. Solutions computed by TVD scheme with van Leer's limiter for $M_\infty = 0{\cdot}96$ using 90×40 grids

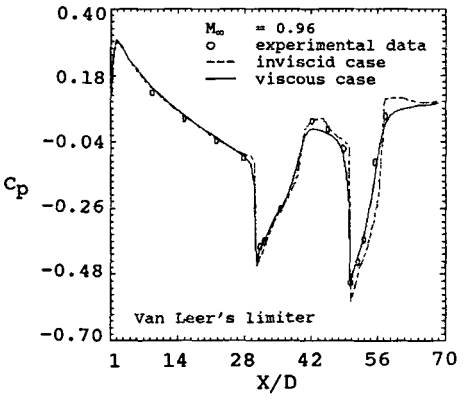

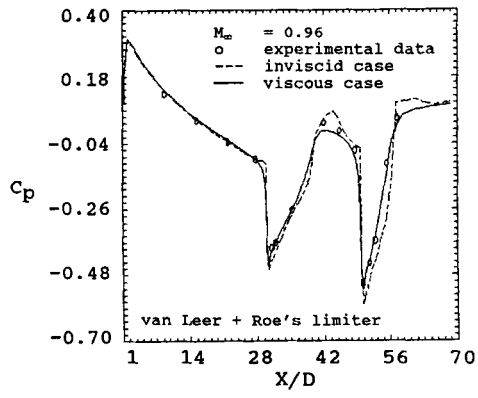

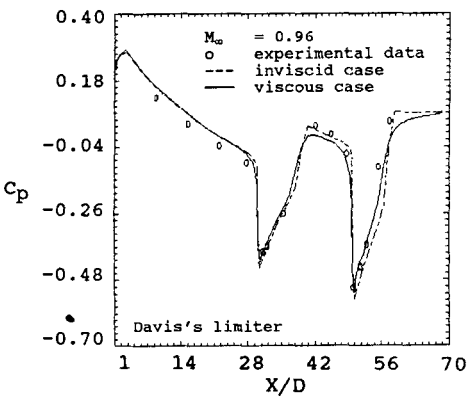

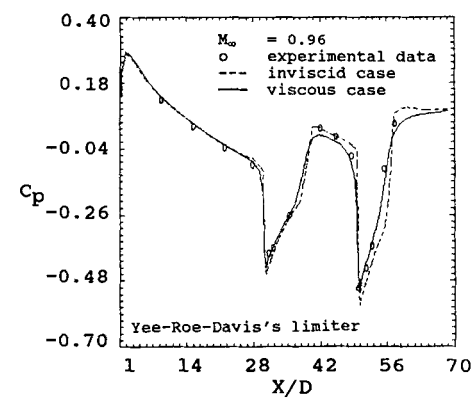

Figure 10. Surface pressure coefficients computed by four TVD schemes for $M_\infty = 0{\cdot}96$ with 70×40 grids

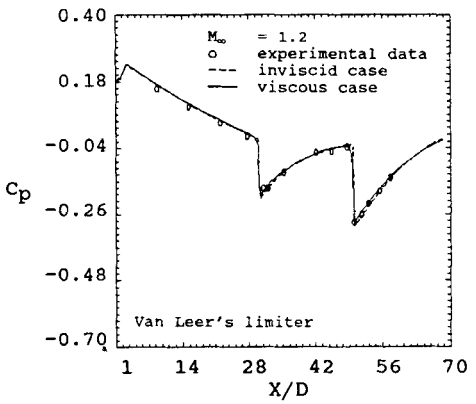

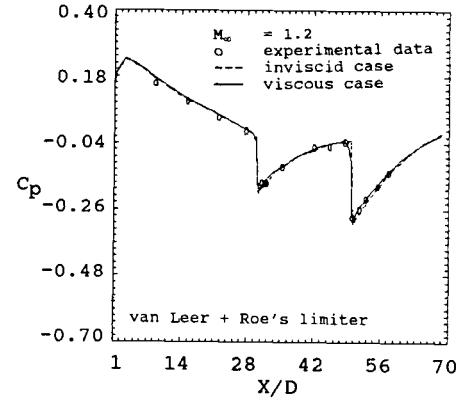

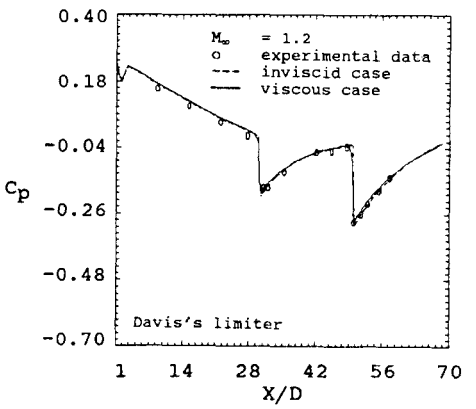

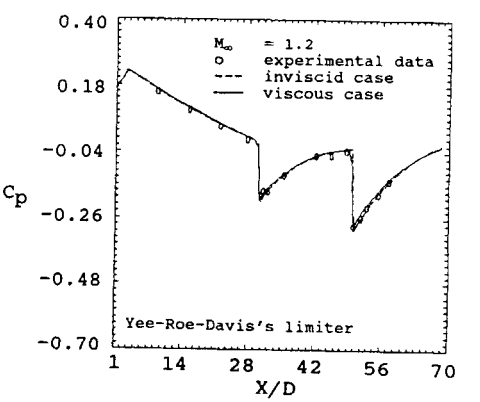

Figure 11. Surface pressure coefficients computed by four TVD schemes for $M_\infty = 1{\cdot}2$ with 70×40 grids

Mach contours of the turbulent flow predicted by the four TVD schemes on this grid system are compared in Figure 10. Qualitatively similar results are observed for all four TVD schemes. However, it is also noticeable that the two upwind schemes are able to yield slightly better agreements between the prediction and the measurement in terms of the pressure coefficient. The symmetric version with a more diffusive limiter, equation (16a), shows the largest discrepancies compared to the measurement. This trend indicates that the two upwind TVD schemes are more grid-insensitive than the symmetric schemes.

3.2. $M_\infty = 1{\cdot}2$

In this case, as the Mach number is increased from $M_\infty = 0{\cdot}96$ to $1{\cdot}2$, a weak oblique shock forms at the nose of the projectile.

Computations on a 70×40 grid system have been conducted for both inviscid and turbulent flows. Figure 11 shows that the computed pressure coefficients using all four TVD schemes are in

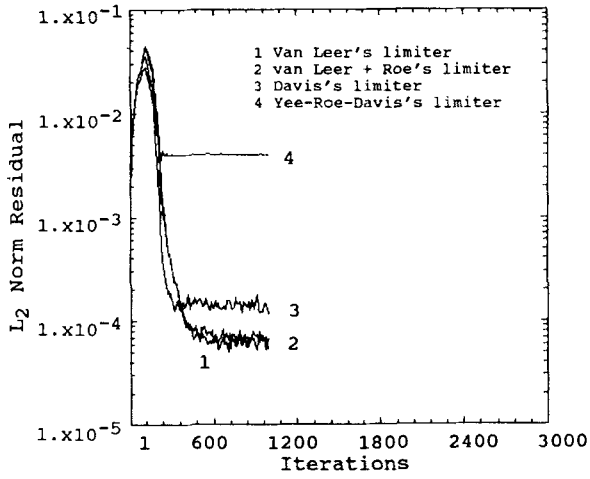

(a) inviscid flow.

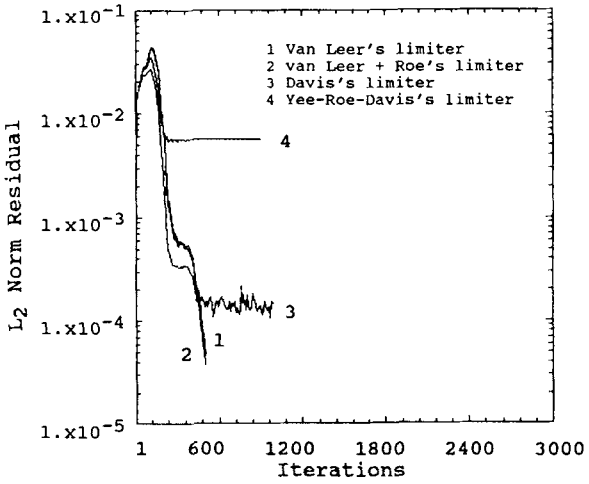

(b) turbulent flow.

Figure 12. Convergence histories of four TVD schemes for inviscid and turbulent flows of $M_\infty = 1{\cdot}2$ with 70×40 grids

excellent agreement with the measurement. For the present flow, no noticeable differences have been identified between the inviscid and turbulent flows for the pressure coefficient. This phenomenon can be largely attributed to the fact that a weak shock forms at the nose of the projectile. Hence, unlike the case of $M_\infty = 0{\cdot}96$ where the shock/boundary layer interaction can substantially modify the wall pressure distribution, the present case is relatively insensitive to the viscous effects. Finally, Figure 12 compares the convergence rates for both the inviscid and turbulent flows. The results are not the same as in the case of $M_\infty = 0{\cdot}96$. First, the convergence rates yielded by the same TVD scheme for both the inviscid and turbulent flows are also very close owing to the relatively small effects of the viscosity. Although all four limiters of the TVD scheme show very comparable convergence rates, the symmetric TVD scheme of Yee–Roe–Davis limiter shows a much higher level of persistent residuals. The other symmetric scheme also shows a somewhat higher level of residuals than the two upwind schemes. The higher levels of residuals are very tolerable here in view of the fact that the solutions predicted by the different schemes are very close. Nevertheless, further investigations are needed to identify and to resolve the difficulty of the symmetric TVD schemes in terms of residual reduction, since it may become more critical for flow of higher incoming Mach number.

4. CONCLUDING REMARKS

A thin layer Navier–Stokes flow code based on the conventional Beam–Warming scheme has been modified to facilitate the adoption of TVD schemes. Four variants of the TVD scheme, namely two upwind flux limiters proposed by van Leer and by Roe and two symmetric flux limiters proposed by Davis and by Yee–Roe–Davis, have been adopted. The results obtained show that all four variants can accurately resolve the shock and flow profiles with fewer grid points than the Beam–Warming scheme. Furthermore, although the computing cost of the TVD schemes are higher than the Beam–Warming scheme for each time step, the higher convergence rates of these schemes make them computationally efficient overall. The combination of high accuracy, good robustness and improved computational efficiency offered by the TVD schemes makes them extremely attractive for computing high-speed flow with shocks. In terms of the relative performances, it is found that for the transonic flow the symmetric schemes converge slightly faster but that the upwind schemes are less sensitive to the number of grid points being employed.

ACKNOWLEDGEMENTS

The authors wish to thank Dr. H. C. Yee of NASA Ames Research Center for providing a listing of her 2D TVD code, which was very helpful for the development of the current research code for the axisymmetric transonic aerodynamic problem. The authors are also grateful to acknowledge the grant of computer time by the National Center for Supercomputing Applications at the University of Illinois at Urbana-Champaign.

REFERENCES

1. P. L. Roe, 'Characteristic-based schemes for the Euler equations', *Ann. Rev. Fluid Mech.*, **18**, 337–366 (1986).
2. P. L. Roe, 'Some contributions to the modelling of discontinuous flows', *Proc. AMS–SIAM Summer Seminar on Large-Scale Computation in Fluid Mechanics*, the American Mathematical Society, Providence, RI, Vol. 2, 163–194, 1985, 27 June–8 July 1983, *Lectures in Applied Mathematics*, Vol. 22, 1985.
3. A Harten, 'A high resolution scheme for the computation of weak solutions of hyperbolic conservation laws', *J. Comput. Phys.*, **49**, 357–393 (1983).

4. A. Harten, 'On a class of high resolution total-variation-stable finite difference schemes', *SIAM J. Numer. Anal.*, **21,** 1–23 (1984).
5. B. van Leer, 'Towards the ultimate conservative difference scheme V: A second-order sequel to Godunov's methods', *J. Comput. Phys.*, **32,** 101–136 (1979).
6. P. Colella and P. R. Woodward, 'The piecewise parabolic method (PPM) for gasdynamics simulations', *J. Comput. Phys.*, **54,** 174–201 (1984).
7. S. Osher, 'Shock modeling in transonic and supersonic flow', in W. G. Habashi (ed.), *Advances in Computational Transonics*, Pineridge Press, Swansea, pp. 607–644, U.K., 1984.
8. H. C. Yee, R. F. Warming and A. Harten, 'Implicit total variation diminishing (TVD) schemes for steady-state calculations', *J. Comput. Phys.*, **57,** 327–360 (1985).
9. H. C. Yee, 'Construction of explicit and implicit symmetric TVD schemes and their applications', *NASA TM-86775*, July 1985; also *J. Comput. Phys.*, **68,** 151–179 (1987).
10. H. C. Yee, 'Upwind and symmetric shock-capturing schemes', *NASA TM-89464*, 1987.
11. S. K. Godunov, 'Finite difference method for the numerical computation of discontinuous solutions for the equations of fluid dynamics', *Math. Sbornik*, **47,** 271–306 (1959); also Cornell Aeronautical Lab. translation.
12. P. L. Roe, 'Approximate Riemann solver, parameter vectors and difference scheme', *J. Comput. Phys.*, **43,** 357–372 (1981).
13. P. L. Roe, 'Numerical algorithms for the linear wave equations', *RAE Technical Report TR-81047*, 1981.
14. P. L. Roe and M. J. Baines, 'Algorithms for advection and shock problems', in H. Viviand (ed.), *Proc. 4th GAMM Conf. on Numerical Methods in Fluid Mechanics*, Braunschweig, Vieweg. Vol. 5 pp. 281–290, 1982.
15. A. Harten and J. M. Hyman, 'A self-adjusting grid for the computation of weak solutions of hyperbolic conservation laws', *J. Comput. Phys.*, **50,** 235–269 (1983).
16. P. K. Sweby and M. J. Baines, 'Convergence of Roe's scheme for the general nonlinear scalar wave equations', *J. Comput. Phys.*, **56,** 135–148 (1984).
17. S. Osher, 'Riemann solver, the entropy condition and difference approximations', *SIAM J. Numer. Anal.*, **21,** 217–235 (1984).
18. S. Osher and S. Chakravarthy, 'Very high order accurate TVD schemes', *The IMA Volumes in Mathematics and Its Applications*, Vol. 2, Springer, New York, 1986, pp. 229–274.
19. H. C. Yee, On the implementation of a class of upwind schemes for systems of hyperbolic conservation laws', *NASA TM-86839*, September 1985.
20. S. F. Davis, 'TVD finite difference schemes and artificial viscosity', *ICASE Report No. 84–20*, 1984.
21. P. L. Roe, 'Generalized formulation of TVD Lax–Wendroff schemes', *ICASE Report No. 84–53*, October 1984.
22. R. M. Beam and R. F. Warming, 'An implicit factored scheme for the compressible Navier–Stokes equations', *AIAA J.*, **22,** 393–402 (1978).
23. M. H. Chen, 'On total variation diminishing schemes for transonic turbulent flow computation', *Ph.D. Thesis*, University of Florida, 1988.
24. T. H. Pulliam and J. L. Steger, 'Implicit finite difference simulations of three-dimensional compressible flows', *AIAA J.*, **18,** 159–167 (1980).
25. C. J. Nietubicz, T. H. Pulliam and J. L. Steger, 'Numerical solution of the azimuthal-invariant thin-layer Navier–Stokes equations', *AIAA Paper 79–0010*, 1979.
26. B. van Leer, 'Towards the ultimate conservation difference scheme II, Monotonicity and conservation combined in a second order scheme', *J. Comput. Phys.*, **14,** 361–370 (1974).
27. B. S. Baldwin and H. Lomax, 'Thin layer approximation and algebraic model for separated turbulent flows', *AIAA Paper 81–1262*, 1981.
28. J. L. Steger, C. J. Nietubicz and K. R. Heavey, 'A general curvilinear grid generation program for projectile configurations', *BRL Memorandum Report MR-03142*, October 1982.
29. L. D. Kayser and F. Whiton, 'Surface pressure measurement on a boattailed projectile shape at transonic speed', *ARBRL-MR-0316*, U.S. Army Ballistic Research Laboratory, Aberdeen Proving Ground, MD, 1982.